Angle-resolved photoemission study of CuI

J. G. Gross,* M. Fliyou, S. Lewonczuk, and J. Ringeissen

*Laboratoire de Spectroscopie et d'Optique du Corps Solide, Université Louis Pasteur 5, rue de l'Université,
67084 Strasbourg Cedex, France*

R. Pinchaux

*Laboratoire pour l'Utilisation du Rayonnement Electromagnétique, Bâtiment 209d,
Université Paris—Sud, 91405 Orsay Cedex, France*

(Received 9 June 1987)

Angle-resolved photoemission is measured on bulk crystals of CuI cleaved *in situ*. A direct transition regime is observed. The shape of three valence bands is given. Secondary electron emission localizes some conduction-band features. The proposed band scheme assumes characteristic transitions which are effectively observed in the optical spectra we had measured previously. The spin-orbit splitting, observed in two valence bands, permits the evaluation of the mixing rate of iodine and copper orbitals.

I. INTRODUCTION

We have performed angle-resolved photoelectron spectroscopy (ARPES) measurements on monocrystals of CuI. These experimental data, combined with those obtained by reflectivity spectroscopy, also performed with synchrotron radiation, permit us to give a definite shape to the band scheme in CuI.

Up to now the particular case of CuI is only considered through systematic studies devoted to the I-VII compounds. From the theoretical point of view, Overhof[1] calculated the band scheme of CuCl, CuBr, and CuI in the Korringa-Kohn-Rostoker (KKR) model, taking into account the spin-orbit coupling.

The first indications for some symmetry points in the valence bands were found by optical measurements, limited to 10 eV, and performed on thin samples of the cuprous halides and their alloys.[2] The photoemission measurements, in the UPS range, on thin layers, confirm the mixing of the 3d Cu^+ and np X^- orbitals and permit the proposition of a general layout of the valence bands.[3] The trends from CuCl to CuI are drawn in the review paper by Goldmann[4] which also reports some data in the x-ray range.

We have previously performed reflectivity measurements up to 30 eV with synchrotron radiation.[5] This range involves transitions from four valence bands to two conduction bands. Interpreted in terms of critical points in the joint density of states, these spectra permit the precise determination of high symmetry points, provided that either the final state or the initial state of a transition is unambiguously located in the Brillouin zone. In a first attempt we tried to find answers to this problem by a systematic study taking into account the similarity of the spectra and their evolution from CuCl to CuI.

CuCl is the most studied cuprous halide. It may be noted, for instance, that two-photon absorption gives the separation between the top of the valence band and the nondispersed component of the 3d Cu^+ band.[6] ARPES measurements on epitaxially grown thin layers, interpreted in terms of the one-dimensional density of states, give the width of the valence bands and some trends about their dispersion.[7] Secondary electron emission also indicates some features about the conduction bands.[8] The reflection spectrum we measured, in addition to these data, permitted us to propose a realistic band structure of CuCl.[9]

In the particular case of CuI, we find the additional data we need to interpret the optical spectrum by performing the ARPES experiments on bulk crystals we report here. The electrical conductivity and the cleaving capability of CuI make these measurements easier than for CuCl. However, from the physical point of view, the large spin-orbit splitting value reveals many structures which complicate the optical spectra. In order to label the different bands we will encounter in the present study, we recall briefly their origin and their ordering in CuCl.

The valence bands result, respectively (from the highest to the lowest), from the hybridization of 3d Cu^+ and 3p Cl^- orbitals, the contribution of the metal orbitals being predominant (VB1), the flat component of 3d Cu^+ orbitals (VB2), the hybridization of 3d Cu^+ and 3p Cl^-, the halogen contribution being now predominant (VB3), and the 3s Cl^- orbitals (VB4).

The conduction bands (CB1) and (CB2) arise, respectively, from 4s Cu^+ and 4p Cu^+ orbitals. In the present study a third band (CB3), has to be considered.

In the following, Sec. II deals with the experimental procedure. The electron distribution curves (EDC's) are presented and interpreted in Sec. III, while in Sec. IV some comments are made about the final states involved in our measurements. In Sec. V we reinterpret some characteristic features of the optical spectra. Finally, the spin-orbit separation, at Γ in VB1 and VB3, is discussed in Sec. VI.

II. EXPERIMENT

The experiments were done at Laboratoire pour l'Utilisation du Rayonnement Electromagnétique (LURE) using the synchrotron radiation emitted by the storage ring Anneau de Collisions d'Orsay (ACO). CuI crystallizes in the zinc-blende structure, the lattice constant being 6.04 Å. The monocrystalline ingots of CuI are prepared in our laboratory by the flux growth method. The high purity of this material was checked by spectrochemical analysis.[10] The crystals to be studied are cut from these ingots.

Their sizes permit four or five cleavages in the high vacuum chamber (10^{-10} Torr) which is also equipped with a low-energy electron diffraction (LEED) facility. The (110) mirrorlike faces present well-defined diffraction patterns which maintain their sharpness during the measurements of the photocurrent. There are no indications for surface reconstruction.

The angle-resolved photocurrent is measured at normal emission. The light is incident at 45°. The spherical electron analyzer has an angular resolution of about 1°. The overall instrumental resolution is estimated to be better than about 0.15 eV in the 15–35 eV range. Charge effects are not observed; this is due to the high electrical conductivity of CuI. Weak structures are positioned with the help of the second derivative in order to keep the precision compatible with the resolution.

III. EDC'S AND VALENCE BANDS

The electron distribution curves are displayed in Fig. 1. The three valence bands are well resolved. In this figure the dispersive peaks related to the different components are connected by dashed lines denoted A to F.

The VB2 valence band, involving the nonmixed $3d$ Cu^+ orbitals, $\Gamma_8^{v_2}$ in the double group notation, dominates the EDC's throughout the photon energy range of our study by a remarkably fixed peak within 0.1 eV. It may be used as the reference for the dispersive features.

In VB1, the C line shows clearly the dispersion of the $\Gamma_7^{v_1}$ component in the Γ-K-X direction. With increasing photon energies we are approaching the Γ point.

For $\hbar\omega = 28 \pm 1$ eV, where the peak is still well resolved, the smallest binding energy is reached and corresponds to the $\Gamma_7^{v_1}$ point according to the band-structure calculation taking into account the spin-orbit splitting.[1] The shoulder, at about 0.6 eV, observed with $\hbar\omega = 28$ eV, towards the lower binding energies, stands for the $\Gamma_8^{v_1}$ point, the maximum of the valence band (VBM). This separation is in good agreement with the spin-orbit splitting $\Delta_{S.O.} = 0.64$ eV at $k = 0$, given by the excitonic spectroscopy.[11] For $\hbar\omega > 28$ eV, this doublet structure turns progressively into a single peak, broadened either by lifetime effects or by instrumental resolution. This observation implies that the separation $\Gamma_8^{v_1} - \Gamma_8^{v_2}$ is about 2.4 eV.

On lowering the photon energy, the peak belonging to the $\Gamma_7^{v_1}$ component is observed for the last time with

$\hbar\omega = 17$ eV where it is at 0.2 eV from the $\Gamma_8^{v_2}$ peak and where it becomes more intense than the $\Gamma_8^{v_2}$ peak.

From 20 to 16.5 eV another remarkable feature is observed: the $\Gamma_8^{v_1}$ component shows the splitting as expected when going towards the zone edge. The low-energy component (the B line) is still observed but in a diffuse manner at 1.2 eV below VBM with $\hbar\omega = 17$ eV. The high-energy component (the A line), nonresolved up to $\hbar\omega = 21$ eV, moves towards 0.6 eV below VBM where it is observed for the last time with $\hbar\omega = 16.5$ eV.

The fact that the three dispersive peaks disappear one after the other when lowering the photon energy indi-
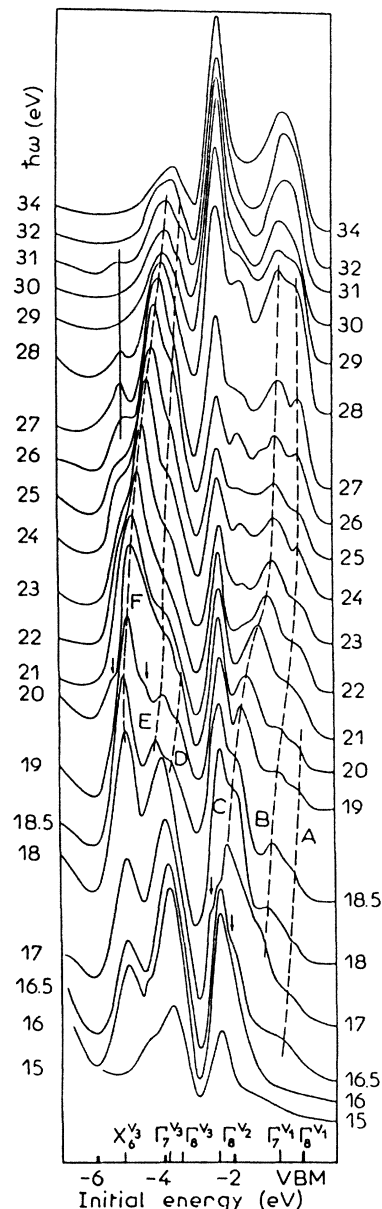

FIG. 1. Angle-resolved photoemission spectra at normal incidence as a function of photon energy. The initial-state energy is referenced to the valence band maximum (VBM). In some curves the arrows indicate secondary emission features.

cates well that the same final state is involved. Below this, if the transitions are no longer observed, we have to assume the existence of a gap in the final-state band or at least a dramatic change of the transition probability which may occur when we are going from one to another final-state band. These remarks suggest that with 16 eV $< \hbar\omega < 28$ eV we are sampling the whole Brillouin zone in the Σ direction. Hence the energies of the three components at $X_7^{v_1}$, $X_6^{v_1}$, and $X_6^{v_1}$ are, respectively, 0.6, 1.2, and 2.2±0.2 eV below VBM.

In VB3 the electronic states have the same symmetry properties as in VB1. Hence the general layout of the different bands should be comparable.

Indeed the dispersion of the $\Gamma_7^{v_3}$ component (the F line) is also clearly observed. This band starts from 3.9 eV below VBM where the transitions are excited at Γ with $\hbar\omega = 31$ eV. The shoulder at 3.5 eV stands for the spin-orbit separation, which is observed for the first time and amounts to 0.4 eV. When lowering the photon energy, the peak belonging to the $\Gamma_7^{v_3}$ component moves away from VBM. For $\hbar\omega = 19$ eV it is at 5.1 eV from VBM. It no longer disperses when $\hbar\omega < 19$ eV. We have to note that the energy reached with $\hbar\omega = 19$ eV corresponds to the nondispersive peak we observe for 24 eV $< \hbar\omega < 28$ eV. Hence this fixed peak, involving probably an umklapp process, stands for the $X_6^{v_3}$ point and with 19 eV $< \hbar\omega < 31$ eV we are sampling the whole Brillouin zone.

The behavior of the $\Gamma_8^{v_3}$ band is more complicated. The dispersion of its lower component (the E line) is observed up to $\hbar\omega = 18.5$ eV where the peak is at 4.2 eV from VBM. The doublet structure, quite evident with 18.5 eV $< \hbar\omega < 20$ eV, gives some indications about the high-energy component of $\Gamma_8^{v_3}$ (the D line). The shoulder observed at 3.8 eV, with $\hbar\omega = 18.5$ eV, is probably significant for the energy of this band at the $X_7^{v_3}$ point. When we go from 18.5 to 18 eV, this doublet structure vanishes suddenly in favor of an intense peak at approximately the energy of the $\Gamma_7^{v_3}$ point. This shows also that we are reaching the zone edge at X. We shall come back to this point later.

Finally, we note a nondispersive structure observed with 23 eV $< \hbar\omega < 29$ eV at 1.7 eV below VBM which cannot be interpreted in terms of band-structure features along Γ-K-X.

At this stage we are able to propose a phenomenological band picture where a linear final-state band scale (the photon energies) supplies the k scale (Fig. 2). This oversimplified view compresses the real band scheme when approaching the zone edge. In this figure the energies of some critical points are also listed.

To complete the description of our experimental results, we note again a very characteristic feature: for $\hbar\omega < 20$ eV a small peak moves through the EDC's. Its shift, with respect to VBM, is equal to the increment of the photon energy; hence, it remains fixed versus the vacuum level and implies a secondary emission process.

The work function ϕ is estimated by the low-energy cutoff and the position of VBM in the EDC's. We obtain $\phi = 6 \pm 0.2$ eV. For instance, the EDC measured
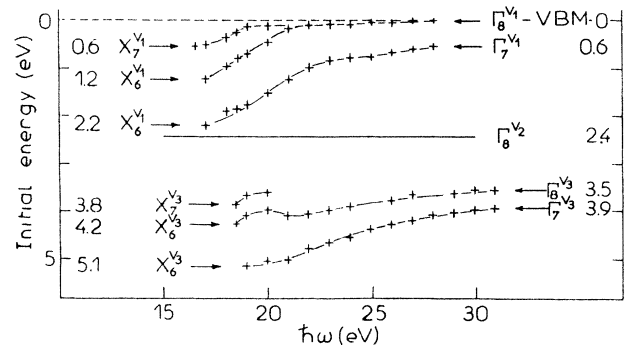

FIG. 2. A qualitative picture of the band scheme; the initial energy of the dispersive peaks or steps are drawn as a function of the photon energy. The energies of the high symmetry points vs VBM are also listed.

with $\hbar\omega = 20$ eV shows that the shoulder marked by an arrow is at 8.5 eV from the vacuum level (Fig. 1).

Two processes are possible to explain the behavior of this feature: the secondary electrons may be emitted either by electron-electron scattering[8] or by Auger emission.[12]

In the Auger process the highest energy available for an emitted electron corresponds to the relaxation of a hole in the $5s$ I$^-$ band, which lies at 10.8 eV from VB2 (Ref. 3) and 13.2 eV from VBM. This energy is not high enough to eject an electron at 14.5 eV above VBM. Consequently, the observed structure is due rather to electron-electron scattering and defines a maximum of the density of the conduction states at 8.5 eV above the vacuum level. The problem of the final states involved in our measurements will be discussed in the following.

IV. FINAL STATES

In numerous cases for metals as well as for semiconductors, the free-electron model applies for the description of the final states for photon energies extending typically from 25 to 100 eV. This approximation is quite reasonable because the crystal field may be considered as a small perturbation.[13]

At smaller energies of photons, real final-state bands may be expected. Sometimes they are described with a "nearly-free electron" model involving an effective mass.[14]

The high symmetry point at 14.5 eV above VBM, as revealed by the small peak moving through the EDC's with varying photon energies, is a first indication that real bands may be involved in our measurements. In order to characterize the shape of these bands we have studied more extensively the secondary electron emission.

In Fig. 3 we represent the EDC's near the low-energy cutoff, measured with an incident photon energy of 40 eV. This emission is produced by electrons which have been excited by electron-electron scattering processes from the valence band into high-lying conduction states. These electrons are then collected preferentially around high symmetry points above the vacuum level.[8] As the electrons are collected at normal emission from the (110)
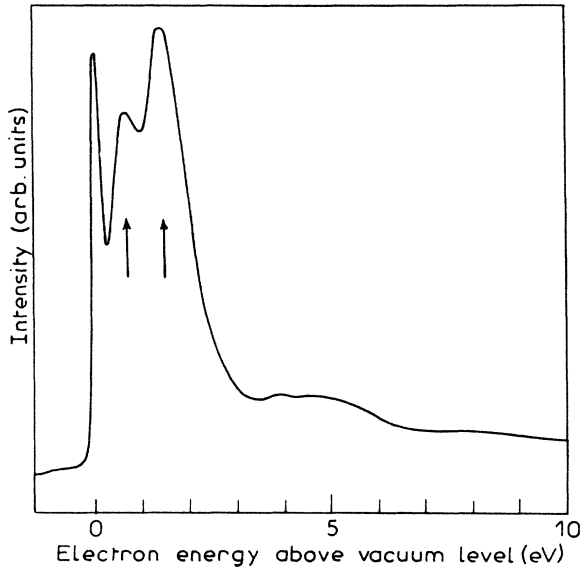
FIG. 3. Secondary electron emission near the low-energy "cutoff" with $\hbar\omega = 40$ eV. Two prominent features (indicated by arrows) above the vacuum level are observed.

face of a monocrystal, the peaks in the secondary electron distribution are directly correlated to critical points along the Γ-K-X direction. The positions of such peaks do not shift, with respect to the vacuum, with variable photon energy.

According to the facts that the fundamental gap, given by the excitonic spectroscopy, is at 3.1 eV and that the width of the first conduction band is less than 2 eV, as expected by band calculations,[1] the structures observed are related to critical points in the second conduction band, the $4p$ Cu^+ one. Hence we associate the structures at 0.6 and 1.5 eV from the cutoff, respectively, to the $X_6^{c_2}$ and $\Gamma_{7,8}^{c_2}$ points which in turn are, respectively, at 6.6 and 7.4 eV above VBM with an indetermination of about 0.3 eV, due in part to the evaluation of the work function.

In our experiment this band is concerned only with transitions smaller than 15 eV when they are excited from VB1 and smaller than 18 eV when they are excited from VB3. In order to explain the experimental data for higher photon energies, we have to consider a third conduction band.

First we shall draw attention to the remarkable behavior of the experimental features belonging to VB3 in the 18–20 eV range.

The doublet structure of the $\Gamma_8^{v_3}$ component is still observed for $\hbar\omega = 18.5$ eV. There is a strong discontinuity at $\hbar\omega = 18$ eV: instead of the doublet we observe a single intense peak whose position, at 3.9 eV below VBM, does not correspond to one of the two components of the doublet but is in agreement with the energy of the $\Gamma_7^{v_3}$ peak for $\hbar\omega = 31$ eV, in other words for $k = 0$.

On the other hand, the peak involving the $\Gamma_7^{v_3}$ component of VB3 disperses up to $\hbar\omega = 19$ eV. Towards lower photon energies it remains fixed at an energy already characterized by a weak peak observed with 24 eV

$< \hbar\omega < 28$ eV. We have attributed this peak to the $X_6^{v_3}$ point at 5.1 eV below VBM.

Hence for $\hbar\omega < 18$ eV the EDC's show two intense peaks which stand, respectively, for the Γ and X symmetry points. This is just what we expect for normal emission when the one-dimensional density-of-states model applies to transitions having their initial states in VB3.

Therefore, our measurements show that the direct model applies up to 19 eV before it changes suddenly to the one-dimensional density model.

It is very interesting to note that this change arises when the final states of the optical transitions go through the critical point $X_{6,7}^{v_2}$ we have localized in the conduction band at 14.5 eV above VBM. This means that we are going from one final-state band to another and that the mixing rate, speaking in terms of atomic orbitals, is strong enough to suppress a gap higher than about 0.5 eV, which is the resolution of the final states in our study (i.e., the photon energy increment). This remark also confirms that the $4p$ Cu^+ conduction band extends up to 14.5 eV above VBM. The direct transition regime we observe for higher photon energies requires some comments.

The dispersion of the Γ_7 component of VB1 as well as of VB3, needs a final-state band extending from the $X_{6,7}^{c_2}$ point, at 14.5 eV above VBM, to the Γ point which has to be at about 27 eV above VBM.

If the free-electron model applies, the transitions involved in the dispersive part of our study have to be located in the extended zone scheme with $\Gamma KX < k_\perp < 2\Gamma KX$. We can estimate the inner potential E_0 of this model with the help of the relation $E = \hbar^2 k^2 / 2m - E_0$, E and E_0 being referenced to VBM. A final state at Γ $(k_\perp = 2\Gamma KX)$, for a transition originating from the $\Gamma_7^{v_3}$ component $(E = 27$ eV) implies $E_0 = 6$ eV. In the same frame, transitions at X should then have their final states at 2.2 eV above VBM. Experimentally, we have already seen that in these transitions the final states at about 14.5 eV are involved. Hence we may conclude that the free-electron model is not relevant in the present case.

As already pointed out,[4,15] two maxima appear in the $2p$ Cl^- absorption spectrum of CuCl reported by Sato et al.:[16] they are at about 16 and 23.5 eV above VBM. Hence the assumption that in CuI a conduction band extends from 14.5 to 27 eV above VBM becomes quite reasonable.

In this context, our results should be compared with the ARPES measurements performed by Goldmann et al.[7] on monocrystalline thin layers of CuCl with photons of 21 eV and interpreted with the help of the one-dimensional density-of-states model. This interpretation is fully consistent with our observation that this model applies to CuI with photons smaller than 18 eV. Actually, it is quite probable that in CuCl the final states of the transitions excited from the Γ_7 component of VB3, with photons of 21 eV, are already in the $4p$ Cu^+ final-state band.

Now arises the question why the direct model transforms into the one-dimensional density model when the final states are going from one conduction band to

another.

The ARPES measurements reported in the past show that it is often difficult to predict whether one model or another would be predominant in a specific case. For III-V semiconductors, at least for $\hbar\omega > 25$ eV, the direct transition model applies, whereas for the lead chalcogenides the band mapping is obtained in the one-dimensional density-of-states model using photons of 35 eV for PbSe (Ref. 17) and photons of 21 eV for PbS, PbSe, and PbTe.[18]

The relative importance of the two models is governed by the relaxation of the $k_\perp$ conservation. It has been shown that in the ideal case the $k_\perp$ conservation should be total when an infinite number of unit cells, in different layers, contribute to the photocurrent. It becomes completely relaxed when the mean free path, or the escape length of the photoelectrons we measure in the vacuum, becomes smaller than the unit cell.[18] Hence the $k_\perp$ relaxation depends essentially on the positions of the sites, with respect to the surface, where the photoelectrons are excited in the optical transition. The smaller the absorption coefficient, the higher the probability that we may collect electrons excited far from the surface. In this way the degree of k conservation is connected with the matrix elements of the optical transitions.

These simple considerations show that it is quite possible that we are going from one regime to another as far as real final states are concerned. A quantitative evaluation needs a precise band structure which is not available up to now.

The present study helps us to propose the overall shape of three conduction bands above the vacuum level defined by some critical points at Γ and X. They are resumed in Fig. 4. In this figure, with regard to the lack of the true analytical form of the third conduction band involved in the direct transition regime, the valence bands are represented by a phenomenological plot deduced from Fig. 2. With the help of this scheme we are able to interpret the most important features of the optical spectra.

V. COMPARISON WITH OPTICAL SPECTRA

The optical spectra reproduce the joint density of states integrated in the whole Brillouin zone. Here we limit ourselves to check that the most characteristic features that we expect from the one-dimensional band scheme (Γ-X) proposed accordingly to our photoemission study, are effectively observed in the optical spectra. In Fig. 5 we show the reflection spectra of CuI, between 4.5 and 30 eV, we had measured in a previous study.[5]

We assume that the intra-atomic transitions, allowed in the dipolar approximation, are intense. Following this idea, transitions between VB2 ($3d$ Cu^+) and CB2 ($4p$ Cu^+) are expected to give rise to pronounced experimental features. In our scheme the $\Gamma_8^{v_2} \rightarrow \Gamma_8^{c_2}$ transition amounts to 9.9 eV. It corresponds remarkably well to the 9.9 eV peak observed in the optical spectra. Moreover, this peak appears clearly in the reflection spectra of the whole sequence of the CuX: at 12.07 eV in CuCl
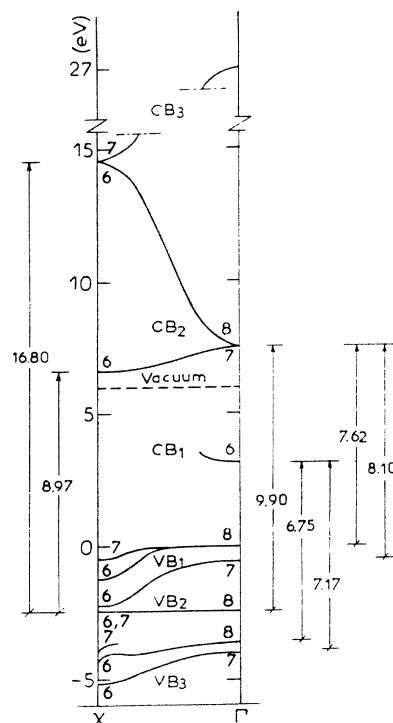

FIG. 4. Band scheme in the Γ-X direction and optical transitions. The conduction bands are presented by an arbitrary plot connecting the high symmetry points.

it has already been attributed to the same transition by Gross.[15]

For the $X_{6,7}^{v_2} \rightarrow X_6^{c_2}$ transition the present band scheme involves an energy of 9 eV: indeed we observe a well-defined peak at 8.97 eV. Finally, the more diffuse structure we locate between 16.8 and 17.35 eV in the second derivative of the optical spectra corresponds to the $X_{6,7}^{v_2} \rightarrow X_{6,7}^{c_2}$ transition that the proposed band scheme fixes at 16.9 eV.

This remarkably good agreement between optical and photoemission spectra confirms well the shape of the $4p$ Cu^+ conduction band.

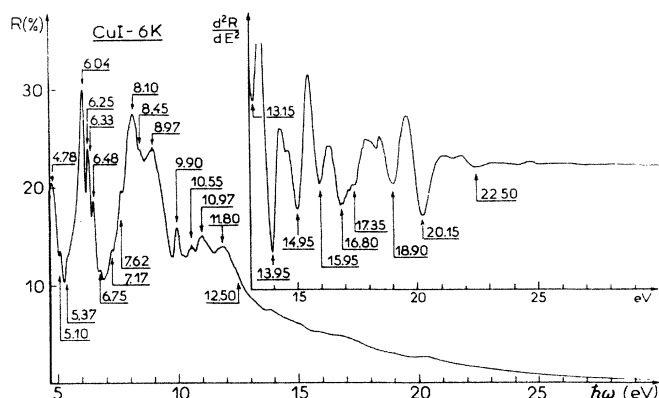Other characteristic features, involving transitions at

FIG. 5. Reflection spectrum measured on bulk crystals with synchrotron radiation (Ref. 5).

Γ from VB1 or VB3, may be easily localized. For instance, referring to Fig. 4, we expect that the absorption between VB3 and CB1 should start at about 6.9 eV. Indeed two features are observed at 6.75 and 7.17 eV. They are related to $\Gamma_8^{v3} \rightarrow \Gamma_6^{c1}$ and $\Gamma_7^{v3} \rightarrow \Gamma_6^{c1}$ and confirm that the spin-orbit splitting in VB3 is near 0.4 eV. In the same manner, though their relative intensities are not known, transitions at Γ between VB1 and CB2 are expected at about 7.4 and 8.1 eV. They are confirmed optically by the step at about 7.6 eV and the peak at 8.1 eV.

This comparison shows essentially that the final states we propose to interpret our photoemission measurements, lead to characteristic transitions which are effectively observed in the optical spectra.

VI. SPIN-ORBIT SEPARATION

The particular band configuration of the CuX, in regard to other isoelectronic compounds, like III-V compounds, has been suggested by Cardona taking into account the behavior of the spin-orbit splitting $\Delta_{S.O.}$, in the excitonic spectra, through the sequence CuCl-CuI.[2] The experimental trends were reproduced by the estimation of the mixing rate, at Γ, of np X^- and $3d$ Cu$^+$ orbitals. For this estimation, the atomic spin-orbit splittings in the zinc-blende structure were obtained by multiplying the one electron atomic splitting by 1.5.

In a more rigorous approach, Song expresses the $\Delta_{S.O.}$ value by the relation[19]

$$\Delta_{S.O._1} = \tfrac{3}{2}(a^2\Delta_p' - b^2\Delta_d') + \frac{3}{2}\frac{b^2\Delta_d'}{\Gamma_8^{v1} - \Gamma_8^{v2}} ,$$

Δ_p' and Δ_d' are the atomic spin-orbit splittings of the halogen and metal ion, respectively, normalized to the unit cell. The second term of this relation expresses the interaction of the Γ_8^{v2} and Γ_8^{v1} levels. The normalizing coefficient O is given by

$$O = a^2 + b^2 + 2abR ,$$

a^2 and b^2 are the mixing rate at Γ of the wave functions, R is the overlapping integral with

$$a^2 + b^2 = 1 \quad \text{and} \quad \Delta_p' = \frac{\Delta p}{O}, \ \Delta_d' = \frac{\Delta d}{O} ,$$

Δ_p and Δ_d are the atomic spin-orbit splitting, respectively, 0.94 and 0.1 eV.[2] The same relation applies for $\Delta_{S.O._3}$ in VB3, where a^2 and b^2 are inversed, the mixing rate being complementary, at Γ in the two valence bands.

$\Delta_{S.O._n}$ being now determined in the two valence bands, we can calculate a^2 and b^2 neglecting in a first approximation the interaction term. We find $a^2 = 0.6$ and $b^2 = 0.4$.

Hence at the Γ point, the participation of iodine wave functions amounts to 60% in VB1 and 40% in VB3. This approach implies $\Delta_p' = 0.77$ eV and $\Delta_d' = 0.08$ eV.

A rough estimation of the interaction term shows that this effect should be negligible: the interaction with Γ_8^{v2} tends to increase the experimental splitting by about 0.25×10^{-2} eV in VB1 and to reduce it by about 0.38×10^{-2} eV in VB3.

The percentage of iodine orbitals in VB1 is somewhat higher than those obtained by the excitonic spectroscopy, 50% (Ref. 2) or by the evaluation of the partial densities of states in photoemission experiments, 45%.[3]

VII. CONCLUSION

The ARPES measurements show a direct transition regime for final states lying higher than 14.5 eV above VBM and permit the determination of the shape of three valence bands. A real final-state band is assumed. The bottom of this band and critical points in the $4p$ Cu$^+$ conduction band are localized by the secondary electron emission. For final states in the $4p$ Cu$^+$ band, the one-dimensional density-of-states model applies. The interpretation of the ARPES measurements are in good agreement with the optical spectra we measured previously. For the first time the spin-orbit splitting in the third valence band is observed. It permits us to evaluate, in a more precise manner, the mixing rate of halogen and metal orbitals.

*Deceased.
[1]H. Overhof, Phys. Status Solidi B 97, 267 (1980).
[2]M. Cardona, Phys. Rev. B 129, 69 (1963).
[3]A. Goldmann, J. Tejeda, N. J. Shevchik, and M. Cardona, Phys. Rev. B 10, 4388 (1974).
[4]A. Goldmann, Phys. Status Solidi B 81, 9 (1977).
[5]J. G. Gross, S. Lewonczuk, M. A. Khan, and J. Ringeissen, Solid State Commun. 36, 907 (1980).
[6]D. Frohlich and H. Volkenandt, Solid State Commun. 43, 189 (1982).
[7]D. Westphal and A. Goldmann, J. Phys. C 15, 6661 (1982).

[8]A. Goldmann and D. Westphal, J. Phys. C 16, 1335 (1983).
[9]S. Lewonczuk, J. G. Gross, J. Ringeissen, M. A. Khan, and R. Riedinger, Phys. Rev. B 27, 1259 (1983).
[10]C. Schwab and A. Goltzené, Prog. Cryst. Growth Charact. 5, 233 (1982).
[11]J. Ringeissen and S. Nikitine, J. Phys. (Paris) Colloq. 28, C3-48 (1967).
[12]W. Pong and S. K. Okada, Phys. Rev. B 20, 5400 (1979).
[13]T. C. Chiang, J. A. Knapp, M. Aono, and D. E. Eastman, Phys. Rev. B 21, 3513 (1980).
[14]N. B. Brookes, D.S.-L. Law, T. S. Padmore, D. R. Warbur-

ton, and G. Thornton, Solid State Commun. **57**, 473 (1986).

[15]J. G. Gross, thesis, Université de Strasbourg, 1983 (unpublished).

[16]S. Sato, T. Ishii, I. Nagakura, O. Aita, S. Nakai, M. Yokota, K. Ishikawa, G. Matsuoka, S. Kono, and T. Sagawa, J. Phys. Soc. Jpn. **30**, 459 (1971).

[17]P. Thiry, R. Pinchaux, G. Martinez, Y. Petroff, J. Lecante, J. Paigné, Y. Ballu, C. Guillot, and D. Spanjaard, Solid State Commun. **27**, 99 (1978).

[18]T. Granke, L. Ley, and M. Cardona, Phys. Rev. B **18**, 3847 (1978).

[19]K. S. Song, J. Phys. Chem. Solids **28**, 2003 (1967).